Fabrication and Investigation of the Structural, Morphological and Optical Properties of Iron Oxide by Thermal Evaporation Technique and Antibacterial Applications

Shaymaa. A. Mukheef¹, Fouad Sh. Hashim², Khalid Haneen Abass³

1, 2, 3 Department of Physics, College of Education for Pure Sciences, University of Babylon, Iraq

E-mail: shamaa.abdulall.pure298@student.uobabylo.edu.iq pure.foaad.shakir@uobabylon.edu.iq, Pure.khalid.haneen@uobabylon.edu.iq

Abstract

In this paper, thermal evaporation technique were used to prepared iron (Fe) nanofilms deposited on glass substrates. The characterization of the nanofilms by X-ray diffraction (XRD) confirmed the formation of hematite phase for crystalline tetragonal structure (γ -Fe2O3) and maghemite hexagonal crystal structure (α -Fe2O3) at annealing temperature of 200oC, 300oC and 400oC for 2 hours. The average crystallite size increased with increasing annealing temperature. Atomic force microscope (AFM) images of iron oxide nanofilms show a high surface homogeneity in which the distribution of crystalline granules is uniform. Scanning electron microscope (SEM) images showed that the assemblies of nanoparticles in the form of a flowers are spread on the nano surface, which are a candidate for energy storage applications. The optical properties results show that transmittance increase with increasing annealing temperature. The allowed direct optical energy gap (Egopt) decreased with increasing annealing temperature. The optical constants such as absorption coefficient, extinction coefficient, refractive index and real and imaginary parts of dielectric constant also were studied from the studied properties, the prepared films were suitable for optical devices and antibacterial application.

Keywords: Iron oxide, annealing temperature, Nanofilm, AFM, optical properties.

1. Introduction

Recently there has been a renewed interest in research of iron oxide nanoparticles in order to exploit their magnetic properties for recording media, gas sensors, bioprocessing, magnetic refrigeration, ferrofluids, and so on [1]. There are eight different iron oxides that are well known in nature, among them magnetite (Fe3O4), maghemite (γ-Fe2O3) and hematite (α -Fe2O3) shows the unique magnetic properties and they have different polymorphic forms and undergo temperature induced phase transition. Magnetite and maghemite are ideal materials for industrial and biomedical applications. Both have reusable advantage over other iron oxides due to their unique magnetic, catalytic and biochemical properties [2-4]. iron oxide nanoparticles were created using a variety of techniques, including co-precipitation of ferrous/ferric salts [5], thermal degradation of hydrazinated iron(II) oxalate [6], microemulsion [7], sol-gel syntheses [8], and hydroxylation and pyrosol [9]. The current work deals with the synthesis of iron oxide nanofilms from Iron nanoparticles and the study of their structural, morphological and optical properties under influence of annealing temperature.

2. Experimental

2.1 Purification of iron oxide nanofilms

Thermal evaporation system (Edward C-306) was used to prepare iron nanofilms deposited on glass substrate. As source materials for the molybdenum boat, 99.9% pure iron powder was used. The chamber was evacuated to a

pressure of 10-6 mbar. The distance between the source and the substrate was approximately 15 cm, and the nanofilms were annealed at 200 oC, 300 oC and 400 oC for 2 hours.

2. Descriptions

The X-ray diffraction using SHIMADZU (XRD-6000) which investigate structural properties. The Scanning Electron Microscope (SEM) (LEO 1530) and Atomic Force Microscope (AFM type (Aa3000 SPM)) was used to recognize the surface topography of the deposited iron oxide nanofilms. The UV-Visible spectrophotometer (Shimadzu UV1650 PC, Phillips, Japanese company) was considered, to record the transmission in the range of the wavelength (190-1000) nm at RT.

2. Results and Discussion

The X-ray diffraction pattern of pure iron nanofilms as-deposited and different annealing temperature 200 oC, 300 oC and 400 oC for 2 hours are shown in figs. (1-4) individually. Fig.(1) display three salient diffraction peaks at 2θ = 41.365o, 48.156o and 64.432o corresponding to miller indices (100), (101) and (102) for crystalline hexagonal structure of Fe taken from the card file data (34-0529). Fig.(2) obtain three salient diffraction peaks at 2θ = 15.577o, 26.288o and 24.378o corresponding to miller indices (103), (116) for crystalline tetragonal structure γ -Fe2O3 (maghemite) taken from the card file data (25-1402) and (012)* for crystalline hexagonal crystal structure α -Fe2O3 (hematite) taken from the card file

Received: 09.06.22, Revised: 10.06.22, Accepted: 19.08.22

data (33-0664) respectively. Fig.(3) display four salient diffraction peaks at $2\theta=16.200$ o, 26.288o, 30.85O, and 24.135o corresponding to miller indices (103),(116) and (206) for crystalline tetragonal structure γ -Fe2O3 taken from the card file data (25-1402), and (012)* for crystalline hexagonal structure α -Fe2O3 taken from the card file data (33-0664) respectively. Fig.(4.4) display three salient diffraction peaks at $2\theta=26.288$ o, 31.198o, and 41.365o corresponding to millers indices (206) and (116) for tetragonal crystal structure γ -Fe2O3 taken from the card file data (25-1402), and (113)* for hexagonal crystal structure α -Fe2O3 taken from the card file data (33-0664) respectively.

Annealing at different temperature in the presence of air leads to oxidation and reveal the mixed phases of iron oxide maghemite and hematite, implying that annealing played a role of a surfactant to some extent and contributed to the increase in crystallization. The average crystallite size (DS) of samples annealed at different temperature was estimated from the peak broadening of diffraction pattern using Scherrer's formula [10].

$DS = 0.94 \lambda / \beta \cos \theta$ (1)

Where β is FWHM in radians.

From such figures it can be seen that the average crystallite size increased with increasing annealing temperature as can be seen in the Table (1). The intensity of peaks decreased with increasing annealing temperature, which mean enhancement of degree of crystallite. Similar behaviour was reported in the researcher [11].

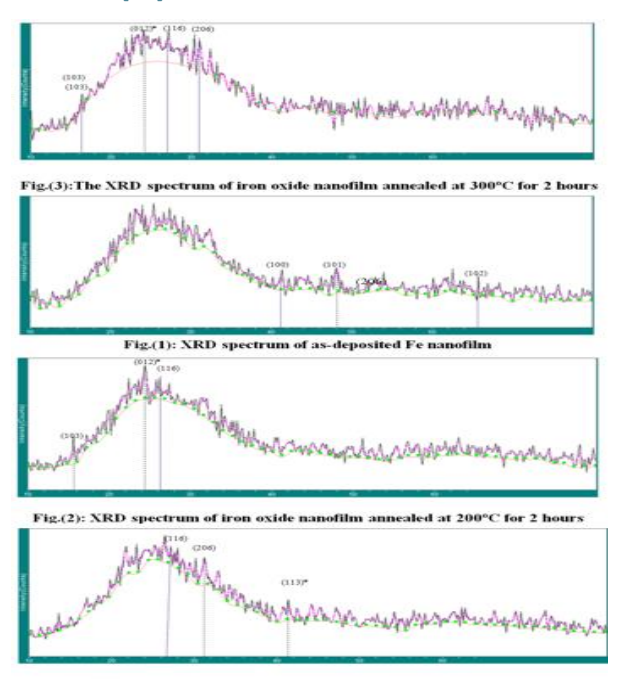


Fig.(4) XRD spectrum of iron oxide nanofilm annealed at 400°C for 2 hours

Table (1): The obtained result from the XRD for prepared nanofilms

Anneali ng with time (hour)	2θ Degr ee		FWHM (degre e)	а	b (Å)	C (Å)	d (Å)	Crystalli te size (nm)	Averag e crystalli te size (nm)	
Λς_	41.76 5	(100)	0.439	2.45	2.45	3.93	2.12	18.12		
As- deposit ed	48.15 6	(101)	0.783	2.45	2.45	3.93	1.84	11	15.12	
	64.43 2	(102)	0.489	2.45	2.45	3.93	1.44	16.24		
	15.57 7	(103)	0.351	8.34	8.34	25.0 2	0.56 8	22.84	18.06	
200°C for 2 h	24.37 8	(012) *	0.568	5.03 5	5.03 5	13.7 4	0.36 4	14.31		
	26.28 8	(116)	0.466	8.34	8.34	25.0 2	3.40 0	17.04		
	16.20 0	(103)	0.351	8.34	8.34	25.0 2	0.56 8	22.84		
300°C for 2 h	24.13 5	(012) *	0.522	5.03 5	5.03 5	13.7 4	0.36 4	15.56	40.20	
	26.28 8	(116)	0.466	8.34	8.34	25.0 2	3.40 0	17.04	18.28	
	30.85	(206)	0.466	8.34	8.34	25.0 2	0.28 6	17.68		
	26.28 8	(116)	0.466	8.34	8.34	25.0 2	3.40 0	17.04		
400°C for 2 h	31.19 8	(206)	0.436	8.34	8.34	25.0 2	0.28 6	18.91	18.43	
	41.36 5	(113) *	0.439	5.03 5	5.03 5	13.7 4	3.93	19.34		

(*)lpha-Fe2O3 (hematite phase) ,and the others γ -Fe2O3(maghemite phase)

The typical AFM scans of the prepared iron oxide nanofilms as deposited and different annealing temperature shown in figs.(5-8). From each figures contain images 3D, Histogram grain and Height distribution. The AFM images show a high surface homogeneity in which the distribution of crystalline granules is uniform which is evident from the convergence of the roughness and root mean square (RMS) values as in Table (2). The white areas of the images indicate that there are set of crystalline granules one on top other, so it can be believe that the adjacent granules come together to form large clusters; therefore, we find that the granules in the white areas are larger than that in other regions. The roughness and root mean square (RMS) values are increased from 1.1 nm and 1.43 nm asdeposited nanofilm to 2.61 nm and 3.4 nm annealed at 400 oC for 2 hours, which is attributed to the fact that the surface diffusion was sufficient due to the deposition temperature. The increase in RMS lead to increase in crystalline growth in vertical direction more than horizontal direction. The values of ten point height confirm the roughness and RMS results. Similar behaviour was reported in [12, 13].

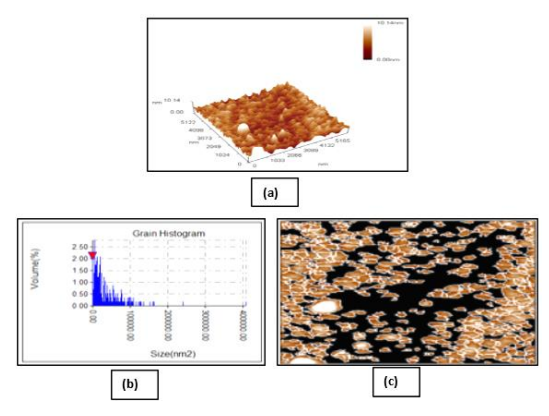


Fig.(5): AFM images of iron oxide nanofilms asdeposited for a)3D, b) Histogram grain and c) Height distribution with data report

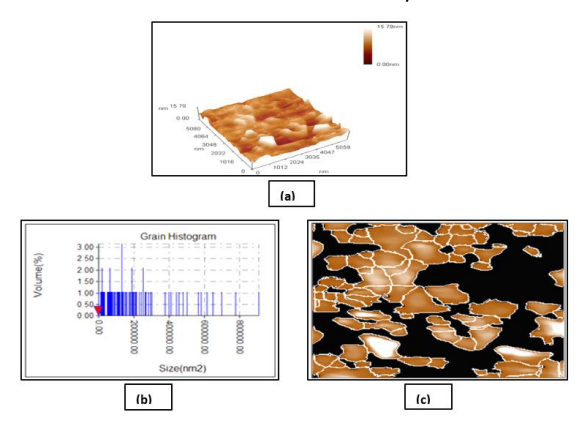


Fig.(6): AFM images of iron oxide nanofilms annealing at 200°C for 2h a) 3D, b) Histogram grain and c) Height distribution with data report

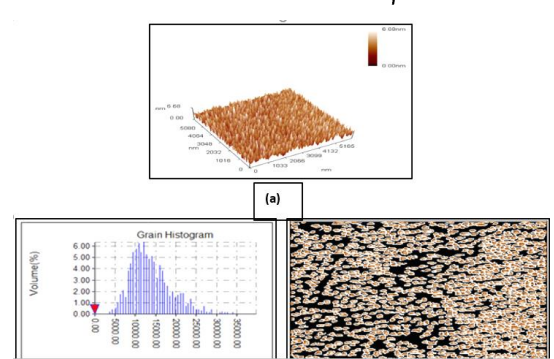


Fig.(7): AFM images of iron oxide nanofilms annealing at 300°C for 2h: a) 3D, b) Histogram grain and c) Height distribution with data report

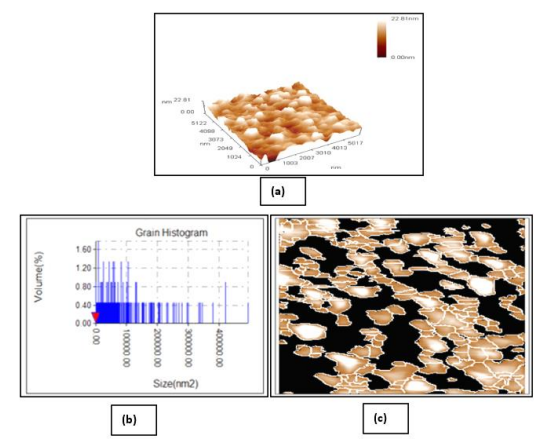


Fig.(8): AFM images of iron oxide nanofilms annealing at 400oC for 2h: a) 3D, b) Histogram grain and c) Height distribution with data report.

Table (2): AFM of iron oxide with different annealing										
with time Annealing Roughness Root mean Ten point										
Annealing with time (h)	Roughness average (nm)	square (nm)	height	Average Diameter(nm)						
as- deposited	1.1	1.43	8.74	201.9						
200oC for 2h	1.33	1.91	10.1	499						
300oC for 2h	0.806	1.01	6.64	133.9						
400oC for 2h	2.61	3.4	18.2	323.1						

The typical SEM micrographs of the prepared iron nanofilm as deposited and different annealing temperatures are presented in figs.(9-12). Annealing at different temperatures contributed to increase of the average particle sizes. The values of the average particle size of the oxidation mixed phases of iron oxide hematite $\alpha\text{-Fe}_2\text{O}_3$ and maghemite $\gamma\text{-Fe}_2\text{O}_3$ nanoparticles deduced from SEM micrographs and their corresponding XRD agree reasonably well, thus indicating a high degree of crystallinity.

Some special particle shapes can be noted depending on the annealing temperatures, the iron that is prepared appears as a spherical shape as in fig. (9), while the nanofilms that are annealed showed assemblies of nanoparticles in the form of a flowers-like shape of Fe₂O₃ spread on the nanofilm surface as in figs. (10 - 12),which are candidates for energy storage applications.

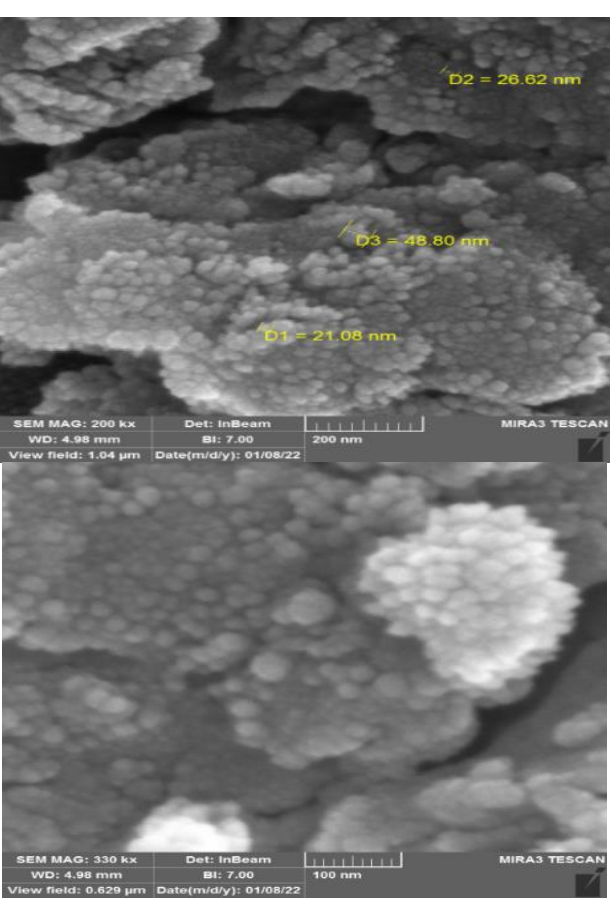


Fig.(9): SEM of as deposited iron nanofilm at different magnification

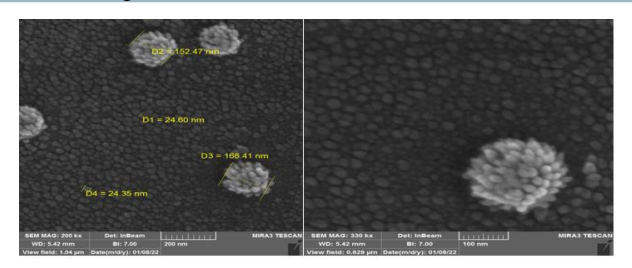


Fig.(10): SEM of iron oxide nanofilm annealed at 200°C for 2 hours at different magnification

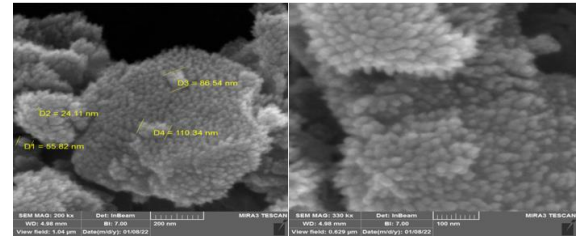


Fig.(11): SEM of iron oxide nanofilm annealed at 300°C for 2 hours at different magnification

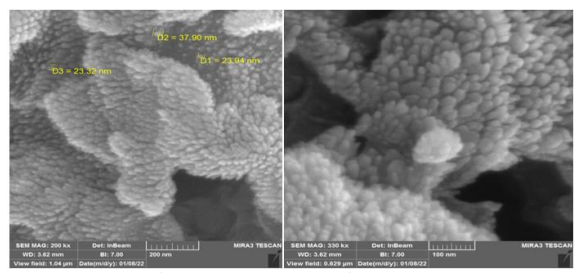


Fig.(12): SEM of iron oxide nanofilm annealed at 400oC for 2 hours at different magnification

The transmittance spectra of Fe nanofilm as-deposited and different annealed temperature as a function of wavelength are shown in figure (13). From this figure, it is obtained that the transmittance reduce with increasing annealing temperature in the UV region and then increase with increasing annealing temperature in the visible and NIR regions. This result is consistent with the findings of the researchers [14].

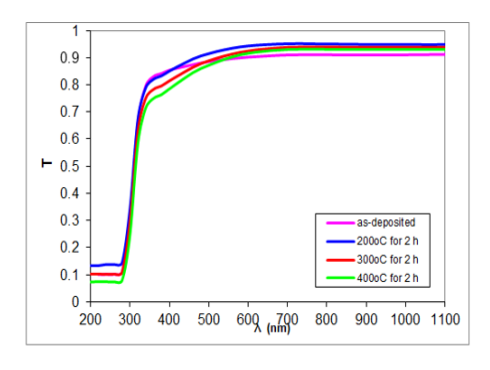


Fig.(13) Transmittance spectra of iron oxide <u>nanofilm</u> with different annealing temperature.

The absorption coefficient (α) has been calculated from the following equation [15]. α = 2.303 (A/d) (2)

Fig.(14) reveal to the absorption coefficient of as a function of wavelength. The value of α is greater than 10^4 cm $^{\text{-}1}$ which mean the direct electron transition happen. It is observed that the α increases with increasing annealing temperature in the UV region and then reduces with increasing annealing temperature in the Vis. and NIR regions. This behaviour related to the absorbance.

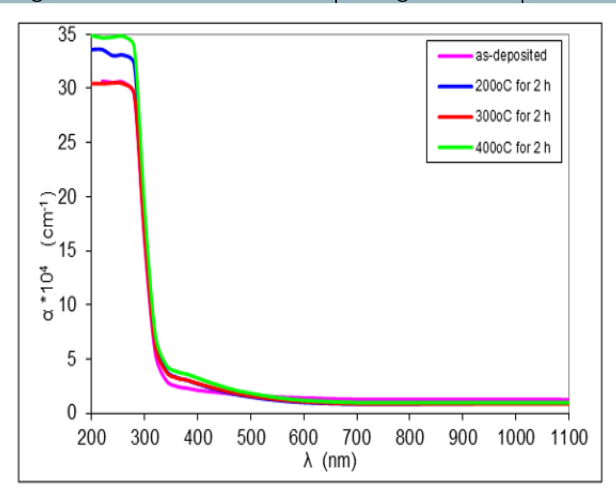


Fig.(14) Absorption coefficient of iron oxide film with different Annealing

Temperature.

The direct optical energy gap (Eg^{opt}) of iron oxide nanofilms was calculated from following equation [16]. $(\alpha hv)^2 \approx hv-E_g$. (3)

Fig.(15) explain the E_g^{opt} of Fe nanofilm as-deposited and different annealed temperature as a function of photon energy (hv). The extrapolation of the straight line to α =0 gives a direct E_g^{opt} equal to 3.48 eV for the as-deposited nanofilms and this value reduce with increasing annealing temperature and takes the values 3.45, 3.39 and 3.33 eV at 200 °C, 300 °C and 400 °C for 2 hours respectively, which is agree with report [17, 18].

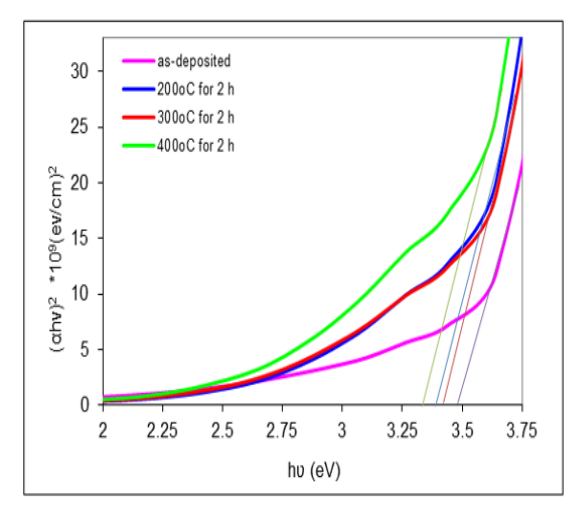


Fig.(15) The direct bad gap of iron oxide <u>nanofilm</u> with different annealing temperature.

The refractive index (n) was calculated from the following equation [13, 19].

$$n = \left(\frac{4R_e}{(R_e - 1)^2} - k^2\right)^{1/2} - \frac{(R_e + 1)}{(R_e - 1)} (4)$$

at which Re denotes reflection.

The refractive index of Fe nanofilm as-deposited and decrease with increasing annealing temperature as in fig.(16). This behaviour due to the decrease in density of nanofilms with increasing annealing temperature

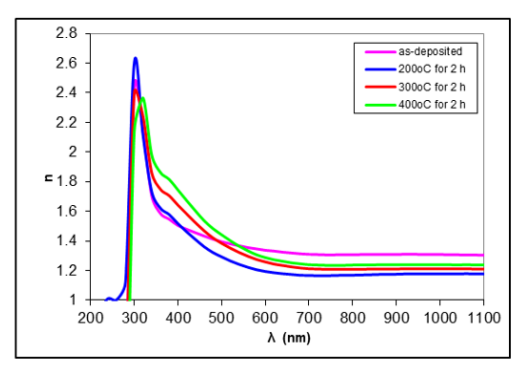


Fig.(16) Refractive index of iron oxide <u>nanofilm</u> with different annealing temperature.

The extinction coefficient (k) were calculated from equations [20, 21]:

$$k=\frac{\alpha\lambda}{4\pi}$$
 (4)

wherever λ is the wavelength.

The extinction coefficient of Fe nanofilm as-deposited increases with increasing annealing temperature in the UV region and then reduces with increasing annealing temperature in the visible and NIR regions as in fig.(17). This behaviour explained by the fact that the k has a similar behaviour to the absorption coefficient.

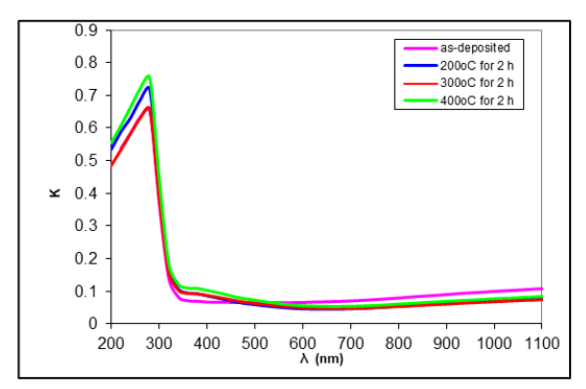
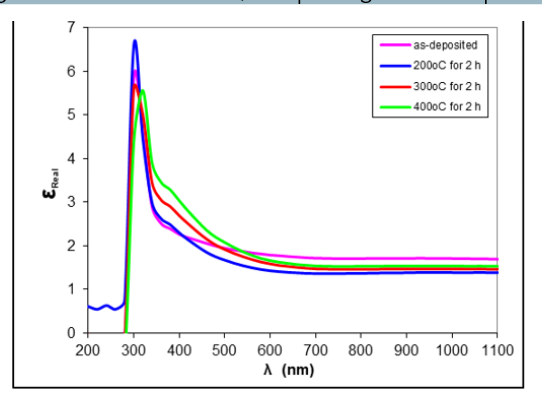


Fig.(17) Extinction coefficient of iron oxide <u>nanofilm</u> with different annealing temperature.

The real and imaginary parts of dielectric constant were calculated by using equations [22].

$$\varepsilon_{\rm r} = n^2 - k^2$$
 (5)
 $\varepsilon_{\rm i} = 2nk$ (6)

Figs.(18,19) explain the real and imaginary parts of dielectric constant of Fe nanofilm as-deposited and different annealed temperature as a function of wavelength. From the fig.(18), it is obtain that the real parts of dielectric constant decrease with increasing annealing temperature. This is due to the real part of dielectric constant depends on refractive index because the effect of extinction coefficient is very small. Fig.(19) explain the imaginary part of dielectric constant increases with increasing annealing temperature in the UV region and then reduces in the Vis. and NIR regions because the imaginary part depends on extinction coefficient especially in the Vis. and NIR regions of wavelength where the refractive index is approximately constant while extinction coefficient increases with the increase of the wavelength.



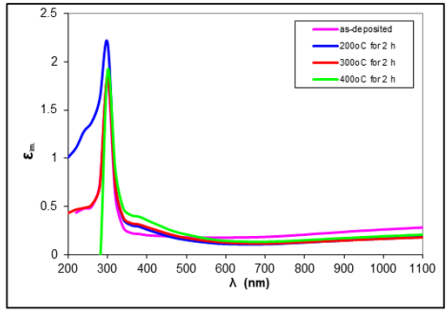


Fig.(19) The imaginary parts of dielectric constant of iron oxide <u>nanofilm</u> with different annealing temperature

3. Conclusion

The characterization of the nanofilms by XRD confirmed the formation of hematite phase for crystalline tetragonal structure (y-Fe2O3) and maghemite hexagonal crystal structure (α-Fe2O3) at annealing temperature. Also the average crystallite size increased with increasing annealing temperature. AFM images of iron oxide nanofilms show a high surface homogeneity in which the distribution of crystalline granules is uniform. SEM images showed that the assemblies of nanoparticles in the form of a flowers are spread on the nano surface, which are a candidate for energy storage applications. The allowed direct optical energy gap (Egopt) decreased with increasing annealing temperature. The optical constants such as absorption coefficient, extinction coefficient and imaginary parts of dielectric constant increased with increasing annealing temperature in the UV region and then reduces with increasing annealing temperature in the Vis. and NIR regions. Refractive index and real parts of dielectric constant decreased with increasing annealing temperature from the studied properties, the prepared films were suitable for optical devices and antibacterial application.

Reference

- 1. Morrish AH. Canted Antiferromagnetism: Hematite. World Scientific, 1994. Available from: https://books.google.com.pk/books?id=E2X8uW8UxmEC
- 2. Cornell RM, Schwertmann U. The iron oxides: structure, properties, reactions, occurrences, and uses. Wiley-vch Weinheim, 2003.

https://doi.org/10.1515/CORRREV.1997.15.3-4.533

- 3. Shatokha V. Iron Ores and Iron Oxide Materials. IntechOpen, 2018. Available from: https://books.google.com.pk/books?id=qXCQDwAAQBAJ
 - . Machala L, Tucek J, Zboril R. Polymorphous

transformations of nanometric iron (III) oxide: a review. Chemistry of materials. 2011;23(14):3255-72. https://doi.org/10.1021/cm200397g

- 5. Jafari A, Shayesteh SF, Salouti M, Boustani K. Effect of annealing temperature on magnetic phase transition in Fe3O4 nanoparticles. Journal of Magnetism and Magnetic Materials. 2015;379:305-12. https://doi.org/10.1016/j.jmmm.2014.12.050
- 6. Rane K, Verenkar V. Synthesis of ferrite grade γ-Fe2O3. Bulletin of Materials Science. 2001;24(1):39-45. https://doi.org/10.1007/BF02704838
- 7. Chin AB, Yaacob II. Synthesis and characterization of magnetic iron oxide nanoparticles via w/o microemulsion and Massart's procedure. Journal of materials processing technology. 2007;191(1-3):235-7. https://doi.org/10.1016/j.jmatprotec.2007.03.011
- 8. Woo K, Lee HJ, Ahn JP, Park YS. Sol–gel mediated synthesis of Fe2O3 nanorods. Advanced Materials. 2003;15(20):1761-4.

https://doi.org/10.1002/adma.200305561

- 9. Herrero E, AS MCN, Vallet-Reg M. I, JL MART I NEZ and JM GONZ ALEZ-CALBET. Solid State Ion. 1997;101:103-213.
- 10. Taupin V, Capolungo L, Fressengeas C, Das A, Upadhyay M. Grain boundary modeling using an elastoplastic theory of dislocation and disclination fields. Journal of the Mechanics and Physics of Solids. 2013;61(2):370-84.

https://doi.org/10.1016/j.jmps.2012.10.001

- 11. Suresh S, Karthikeyan S, Jayamoorthy K. Effect of bulk and nano-Fe2O3 particles on peanut plant leaves studied by Fourier transform infrared spectral studies. Journal of Advanced Research. 2016;7(5):739-47. https://doi.org/10.1016/j.jare.2015.10.002
- 12. Meftah Y, Bekker D, Benhaoua B, Rahal A, Benhaoua A, Hamzaoui A. Post annealing effect on structural and optical properties of (α-Fe2O3) thin films prepared by spray pyrolysis with moving nozzle. Digest Journal of Nanomaterials and Biostructures. 2018;13(2):465-74. Available from: https://www.researchgate.net/publication/325273327
- 13. Ferdous Z, Ullah MS, Hussain S. Temperature and Substrate Effects on the Structural, Morphological, and Optical Properties of Iron Oxide Thin Films Prepared by Spray Pyrolysis Technique. Dhaka University Journal of Science. 2020;68(1):79-85.

https://doi.org/10.3329/dujs.v68i1.54600

- 14. Abass KH, Mohammed MK. Fabrication of ZnO: Al/Si solar cell and enhancement its efficiency via Aldoping. Nano Biomed Eng. 2019;11(2):170-7. https://doi.org/10.5101/nbe.v11i2.p170-177.
- 15. Hadi EH, Sabur DA, Chiad SS, Fadhil N. Physical properties of nanostructured li-doped zro2 thin films. Journal of Green Engineering. 2020;10(10):8390-400. https://www.researchgate.net/publication/346346289
- 16. Tauc J, Menth A, Wood D. Optical and magnetic investigations of the localized states in semiconducting glasses. Physical Review Letters. 1970;25(11):749. https://doi.org/10.1103/PhysRevLett.25.749
- 17. Kumar A, Yadav K. Optical properties of nanocrystallite films of α -Fe2O3 and α -Fe2- xCrxO3 (0.0 \leqslant

- $x \le 0.9$) deposited on glass substrates. Materials Research Express. 2017;4(7):075003.
- https://iopscience.iop.org/article/10.1088/2053-1591/aa75e9/meta
- 18. Ouertani B, Ouerfelli J, Saadoun M, Ezzaouia H, Bessaïs B. Characterisation of iron oxide thin films prepared from spray pyrolysis of iron trichloride-based aqueous solution. Thin Solid Films. 2008;516(23):8584-6. https://doi.org/10.1016/j.tsf.2008.06.015
- 19. Muhammad SK, Taqi NDM, Chiad SS, Abass KH, Habubi NF. Influence of nanostructured nio thin films doped with chrome by using green chemical spray gyrolysis csp. Journal of Green Engineering. 2021;11(2):1287-99. Available from: https://www.researchgate.net/publication/349849455
- 20. Akhavan O. Thickness dependent activity of nanostructured $TiO2/\alpha$ -Fe2O3 photocatalyst thin films. Applied Surface Science. 2010;257(5):1724-8. https://doi.org/10.1016/j.apsusc.2010.09.005
- 21. Sakhil MD, Shaban ZM, Sharba KS, Habub NF, Abass KH, Chiad SS, Alkelaby AS. Influence mgo dopant on structural and optical properties of nanostructured cuo thin films. NeuroQuantology. 2020;18(5):56. https://www.researchgate.net/publication/342335029